Journal of *Marine Science and Engineering*

MDPI

Article

Geomorphological Features and Formation Process of Abyssal Hills and Oceanic Core Complexes Linked to the Magma Supply in the Parece Vela Basin, Philippine Sea: Insights from Multibeam Bathymetry Analysis

Xiaoxiao Ding [1,2], Junjiang Zhu [1,2,*], Yuhan Jiao [1,2], Xinran Li [1,2], Zhengyuan Liu [1,2], Xiang Ao [1,2], Yihuan Huang [1,2] and Sanzhong Li [1,2]

[1] Key Lab of Submarine Geosciences and Prospecting Techniques, Frontiers Science Center for Deep Ocean Multispheres and Earth System, MOE and College of Marine Geosciences, Ocean University of China, Qingdao 266100, China; dingxiaoxiao@stu.ouc.edu.cn (X.D.); jiaoyuhan@stu.ouc.edu.cn (Y.J.); lixinran@stu.ouc.edu.cn (X.L.); liuzhengyuan@stu.ouc.edu.cn (Z.L.); aoxiang@stu.ouc.edu.cn (X.A.); huangyihuan@stu.ouc.edu.cn (Y.H.); sanzhong@ouc.edu.cn (S.L.)

[2] Laboratory for Marine Mineral Resources, Laoshan Laboratory, Qingdao Marine Science and Technology Center, Qingdao 266237, China

* Correspondence: zhujunjiang@ouc.edu.cn

Abstract

Based on the new high-resolution multibeam bathymetry data collected by the "Dongfanghong 3" vessel in 2023 in the Parece Vela Basin (PVB) and previous magnetic anomaly data, we systematically analyze the seafloor topographical changes of abyssal hills and oceanic core complexes (OCCs) in the "Chaotic Terrain" region, and the revised seafloor spreading model is constructed in the PVB. Using detailed analysis of the seafloor topography, we identify typical geomorphological features associated with seafloor spreading, such as regularly aligned abyssal hills and OCCs in the PVB. The direction variations of seafloor spreading in the PVB are closely related to mid-ocean ridge rotation and propagation. The formation of OCCs in the "Chaotic Terrain" can be explained by links to the continuous and persistent activity of detachment faults and dynamic adjustments controlled by variations of deep magma supply in the different segments in the PVB. We use 2D discrete Fourier image analysis of the seafloor topography to calculate the aspect ratio (AR) values of abyssal hills in the western part of the PVB. The AR value variations reveal a distinct imbalance in magma supply across various regions during the basin spreading process. Compared to the "Chaotic Terrain" area, the region with abyssal hills indicates a higher magma supply and greater linearity on seafloor topography. AR values fluctuated between 2.1 and 1.7 of abyssal hills in the western segment, while in the "Chaotic Terrain", they dropped to 1.3 due to the lower magma supply. After the formation of the OCC-1, AR values increased to 1.9 in the eastern segment, and this shows the increase in magma supply. Based on changes in seafloor topography and variations in magma supply across different segments of the PVB, we propose that the seafloor spreading process in the magnetic anomaly linear strip 9-6A of the PVB mainly underwent four formation stages: ridge rotation, rift propagation, magma-poor supply, and the maturation period of OCCs.

Keywords: Parece Vela Basin; detachment fault; abyssal hill; oceanic core complex; seafloor spreading process

check for updates

Academic Editor: Dimitris Sakellariou

Received: 9 July 2025
Revised: 23 July 2025
Accepted: 24 July 2025
Published: 26 July 2025

Citation: Ding, X.; Zhu, J.; Jiao, Y.; Li, X.; Liu, Z.; Ao, X.; Huang, Y.; Li, S. Geomorphological Features and Formation Process of Abyssal Hills and Oceanic Core Complexes Linked to the Magma Supply in the Parece Vela Basin, Philippine Sea: Insights from Multibeam Bathymetry Analysis. *J. Mar. Sci. Eng.* **2025**, *13*, 1426. https://doi.org/10.3390/jmse13081426

Copyright: © 2025 by the authors. Licensee MDPI, Basel, Switzerland. This article is an open access article distributed under the terms and conditions of the Creative Commons Attribution (CC BY) license (https://creativecommons.org/licenses/by/4.0/).

1. Introduction

Oceanic core complexes (OCCs) are seafloor massifs composed of lower crust and upper mantle rocks [1], typically exposed at the ocean floor through the sliding of detachment faults [1–3]. OCCs are important structure units in the mid-ocean ridge system, and research on OCCs plays a key role for understanding mid-ocean ridge spreading, crustal growth, and seafloor structural variations [1–4]. Over the past 45 years, OCCs have been a key window in Earth sciences, inducing extensive attention for lots of geoscientists [1,5–10]. OCCs have been widely and globally found in mid-ocean ridges from moderate spreading to ultra-slow spreading systems. Among them, the "Godzilla Megamullion" discovered in the PVB is the largest OCC to date (Figure 1a) [7]. OCCs have also been identified in other mid-ocean ridge systems, such as the Mid-Atlantic Ridge [1], the Southwest Indian Ridge [8], and the Australian-Antarctic Discordance [11] (Figure 1a). OCCs are typically located at the end part of spreading ridge segments with limited magma supply or found at the junction points of transform faults between adjacent ridges. The seafloor topography of the OCCs shows typical corrugated surface pattern parallel to the spreading direction, exposing ultramafic rocks such as gabbro and peridotite [6–8,11]. The presence of OCCs indicates a weakening of magmatic activity in the specific region during the spreading process [12]. Many early formation models of OCC suggested that the evolution of OCC is closely related to activity of detachment faults (Figure 1b) [1]. In specific regions of mid-ocean ridges, limited or intermittent magma supply determines the formation of long-lived detachment faults [2,3]. Previous studies have shown that magma supply also plays a key role in the formation of OCCs [13–15]. To generate long-lived detachment faults, the magma supply should not be too low. If the magma supply is insufficient, detachment faults cannot persist [16]. The OCCs in the PVB provide an important window for studying the formation of oceanic crust and the generation of the oceanic lithosphere [7]. The formation and evolution of OCCs not only reveal mechanisms of crustal deformation and heat flow transfer but also offer valuable insights into the deep material cycle. This allows for an in-depth exploration of the mechanisms of crustal generation, material sources, and composition variations, furthering our understanding of the role of oceanic crust in crustal evolution [17–19].

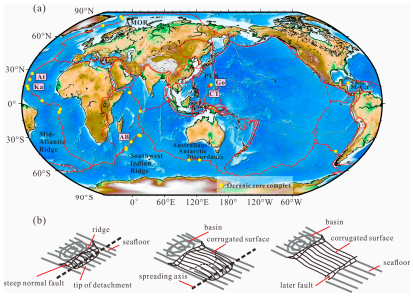


Figure 1. Locations and evolution models of global OCCs. (**a**) Location map of typical OCCs. The yellow dots represent the locations of OCCs (data from [20]). The red triangle marks the location of OCCs found in the "Chaotic Terrain" characterized by rough, isolated, and uplifted domal structures, topped by axis-perpendicular corrugations and accompanied by adjacent deep swales, on the western side of the PVB in this study. (**b**) A 3D schematic evolution models of OCCs under detachment faulting (modified from [1]). The gray lines represent the seafloor (excluding the detachment surface), and the black lines indicate the surfaces of detachment faults and steeper normal faults and both faults exposed at the seafloor and beneath. The interaction between the ridge and the basin leads to fault rotation and bending, forming detachment faults, which are later cut by normal faults. This causes the OCCs to be flat, and the detachment faults become inactive. AB: Atlantis Bank (SW Indian Ridge); AMOR: Arctic segment of Mid-Atlantic Ridge; At: Atlantis Massif (Mid-Atlantic Ridge); CT: Chaotic Terrain; Go: Godzilla Megamullion; Ka-Kane (Mid-Atlantic Ridge); M-Ca: Mid-Cayman spreading center; PVR: Parece Vela Rift.

The tectonic evolution of the PVB is important for geodynamic studies [21,22] and it provides key evidence for understanding magma supply, energy transfer, and lithosphere-asthenosphere interactions. The basin's spreading process and the formation of oceanic core complexes (OCCs) have been an important aspect in deep-sea geological research [7,17,19,23–25]. The formation and evolution of the PVB indicate the combined effects of geological processes, such as subduction, rifting, and seafloor spreading, revealing the complexity of Earth's deep dynamics and crustal evolution [26,27]. Early studies mainly focused on the analysis of seafloor topography and sediment transfer, confirming the existence of the Parece Vela Rift and its spreading history [5,26]. These studies indicated that the formed oceanic crust propagated northward from the rift center. As spreading progressed, the spreading axis became progressively segmented, the spreading rate became slow, and magma supply began to decrease [5,21,26,27]. Later research further explored the geological features of the region, revealing the composition and evolution of oceanic core complexes (OCCs). In 2001, the discovery of the massive "Godzilla Megamullion" at the extinct spreading center of the PVB highlighted the region's OCCs significance [7]. Through several scientific expeditions, researchers conducted detailed analyses of the rock types and deformation processes in the OCCs distribution [7,17,24,28,29]. Although previous studies have provided various theoretical supports for the formation of oceanic core complexes (OCCs) [21,26,27], there is still a lack of information on the fine features of seafloor topography and the changes of OCCs and surrounding seafloor topography at the off-axis "Chaotic Terrain" in the western PVB, including the identification and formation processes of OCCs in the "Chaotic Terrain". Although numerical simulations suggest that the formation of OCCs typically occurs during periods of reduced magma supply [15,30], the relationship between the seafloor topography of the "Chaotic Terrain" in the PVB and deep magma supply remains unclear. Therefore, there is an urgent need for high-resolution bathymetry data and structural analyses to understand the relationship between OCCs and magma supply.

In this study, we processed the high-resolution multibeam bathymetry data acquired in 2023 by the "Dongfanghong 3" vessel and combined these data with magnetic anomaly data to analyze the variations in abyssal hills and OCCs in the magnetic anomaly linear strip 9-6A segment on the western side of the PVB, especially the topographical features of OCCs in the "Chaotic Terrain" of this region. Under a detailed examination of the relationship between seafloor topography variations and magma supply in the PVB, we explore the formation patterns of OCCs in the "Chaotic Terrain" and try to construct the seafloor spreading evolution model for further understanding the diverse seafloor topography variations in this region.

2. Geological Setting

The crustal structure of the PVB is typical of oceanic crust with an average thickness of approximately 5 km [31]. The PVB is located at the southeastern edge of the Philippine Sea Plate with the average water depths of 5000–5500 m (Figure 2a). The basin spans about 700 km in width from the west to the east and 2000 km from the north to the south in length, showing a "spindle" shape, which shows an ellipsoid with narrower ends and a wider center in the whole (Figure 2). The central region of the PVB is defined by a series of north–south oriented discontinuous rhomboidal depressions (Figure 2b), with an average depth of about 6000 m, up to 7000 m locally. These depressions are mainly composed of the Parece Vela Rift [26,27,32]. The spreading process of the PVB was divided into two stages. At the first stage, the E–W direction spreading occurs from 26 to 19 Ma, with a half-spreading rate of 4.4 cm/y. At the second stage, the NE–SW direction spreading occurs from 18 to 12 Ma, with a half-spreading rate of 3.5 cm/y [7,21]. Although the typically higher magma supply

(higher extents of melting) is associated with relatively fast-spreading mid-ocean ridges, it indicates a lower degree of mantle melting in the PVB [7,17]. The seafloor topography, sediment thickness, and magnetic anomaly variations on the eastern and western sides of the PVB show significant asymmetry. At the western side of the PVB, it shows a thinner sediment layer, larger seafloor undulations, and clearly discernible magnetic anomaly linear strips; however, at the eastern side of basin, it presents flatter topography, thicker sediment layer, and blurred or even undetectable magnetic anomaly linear strips [5,26].

Two significant formation events of OCCs occurred during the spreading of the PVB. The first was linked to the appearance of the "Chaotic Terrain", and the second was shown to mark the formation of the massive OCC named "Godzilla Megamullion" when the spreading center was about to cease [7]. The "Chaotic Terrain" was first discovered in 1998 and initially was named as the "Transferred Area" by Okino et al. [21]. They called the anomalous area between two ridge segments a transferred zone and the area between failed rift and inner pseudo fault a transferred lithosphere [21]. Later, it was formally renamed as the "Chaotic Terrain" [7]. In the western side of the PVB, the "Chaotic Terrain" consists of a series of isolated uplift blocks and depressions (Figure 2; yellow dashed line). Magnetic anomaly linear strips 6B and 6C are located across the area [21], and regularly aligned abyssal hills surround the "Chaotic Terrain" with the higher mantle bouguer gravity anomalies (~30 mGal). On seismic reflection profiles, it indicates more pronounced seafloor undulations at the western side of the PVB [12] with a relatively thin crust (~5 km) [31,33].

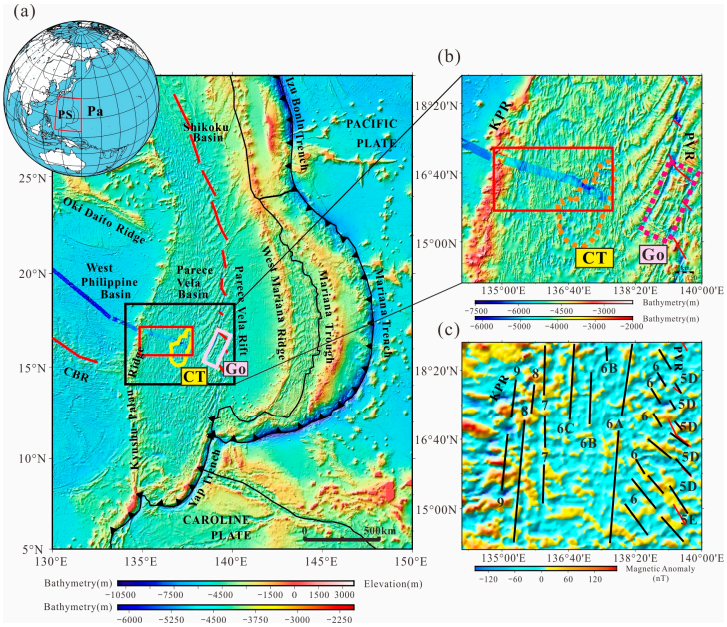


Figure 2. Seafloor topography and magnetic anomaly linear strips in the PVB and its surrounding areas. (**a**) Tectonic units and newly acquired multibeam bathymetry data in the PVB and its surrounding areas. The yellow solid line marks the "Chaotic Terrain" region. The pink box outlines the "Godzilla Megamullion" area, and the red box indicates the study area. The red line represents the two extinct spreading centers within the Philippine Sea Plate. (**b**) Seafloor topography of OCCs identified in the PVB. (**c**) Magnetic anomaly variations and distribution of magnetic anomaly linear strips in the PVB (magnetic anomaly data from [34]). Magnetic anomaly linear strips zones are referenced from [22,35]. CBR: Central Basin Rift; CT: Chaotic Terrain; Go: Godzilla Megamullion; Pa: Pacific Ocean; PS: Philippine Sea; PVR: Parece Vela Rift.

3. Data and Methods

In 2023, high-resolution multibeam bathymetry data were collected by the "Dongfanghong 3" vessel with a hull-mounted Kongsberg EM122 multibeam bathymetry system

in the PVB. During this survey, the ship trackline covers the western side of the PVB, from the Kyushu-Palau Ridge (KPR) to extend eastward to the Parece Vela Rift (Figure 2). The EM122 system operates at a frequency of 12 kHz, with a depth range from 20 to 11,000 m, a maximum swath width up to six times the water depth, and an accuracy of 0.3% of the depth [36]. Multibeam bathymetry data process flowcharts were performed using CARIS HIPS & SIPS 11.1 software [37], focusing on data preprocessing and filtering. Navigation data are corrected, and ship motion anomalies (roll, pitch, and yaw) are edited to enhance data quality. The multibeam bathymetry data are then calibrated using sound velocity profiles derived from temperature and salinity data obtained from several CTD (conductivity, temperature, and depth) stations. After filtering, a preliminary regular grid is created using strip integration and angular weighting methods. Sub-area and strip filtering are applied to remove several anomalies in this survey, similar to filtering step as linear and point anomalies elimination, and by interpolation to eliminate blank area anomalies [38]. The final step is to generate gridded bathymetry data with a 20-meter interval, which were exported in ASCII format. For areas without multibeam bathymetry data in the basin, global bathymetric data GEBCO 2024, with a spatial resolution of 15 arc-seconds and a grid spacing of 500 m [39]. After detailed process, all anomalies are effectively removed and provide a more accurate seafloor topography covered by the multibeam bathymetry data in the PVB (Figure 3).

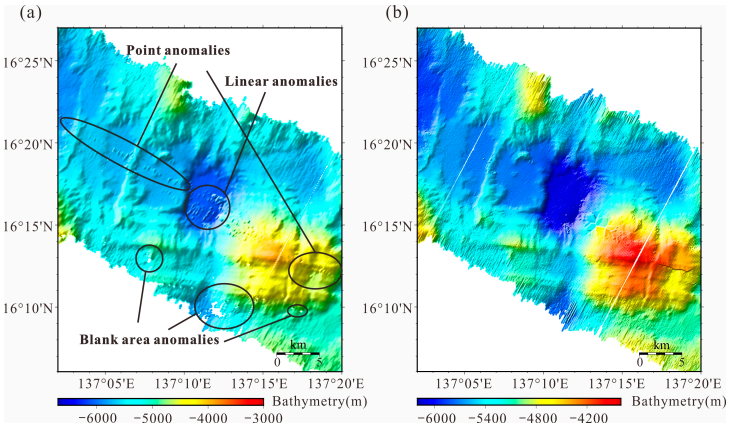


Figure 3. Comparison of seafloor topography before and after multibeam bathymetry data processing. (**a**) Multibeam bathymetry raw data with numerous points as well as linear and blank anomalies before processing. (**b**) Processed multibeam bathymetry data showing true seafloor topography after sub-area and strip filtering steps. All anomalies are removed, and it shows clear topographic features.

In ArcGIS 10.8, the DEM surface tool [40] and the Horn algorithm [41,42] were used to calculate topography slope. Compared to the 4-Cell algorithm, the Horn algorithm provides higher computational accuracy [43]. Compared to the 4-Cell algorithm, the Horn algorithm uses a 3 × 3 neighborhood matrix weighting, improving accuracy, especially in areas with significant terrain changes. The calculation formula is as follows:

$$G(EW) = \frac{[(Z_3 + 2Z_6 + Z_9) - (Z_1 + 2Z_4 + Z_7)]}{8\Delta x} \quad (1)$$

$$G(NS) = \frac{[(Z_1 + 2Z_2 + Z_3) - (Z_7 + 2Z_8 + Z_9)]}{8\Delta y} \quad (2)$$

G(EW) represents the gradient change in the east–west direction, while G(SN) represents the gradient change in the north–south direction. Z_1–Z_9 represent the data points in the 3 × 3 neighborhood matrix.

To further analyze the seafloor slope in the PVB, a 2D discrete Fourier image analysis method [44] was applied for frequency domain processing of the seafloor topography images. Topography of abyssal hills show a high response sensitivity to the 2D discrete Fourier transform, aiding in improving recognition accuracy. In contrast, the flat or chaotic topography of non-abyssal hill areas may lead to erroneous results. To avoid this, eight suitable sampling blocks were selected from the raw data, covering the multibeam strip region. By converting the topography data from these blocks into grayscale slope maps, the images were binarized in subsequent analysis, and spatial orientation information of structural features was extracted using centroid fitting. The aspect ratio (AR) value represents the anisotropy of the image structure and changes on magma supply [44]. When the AR value is greater than 1.5, the spreading direction aligns with the short axis. When the AR value is less than 1.5, the spreading direction tends to be orthogonal to the short axis [44]. The relationship between seafloor slope and magma supply in the PVB will be further discussed in Section 4.

4. Results and Discussion

4.1. Geomorphological Features of Abyssal Hills and OCCs

The collected and processed multibeam bathymetry data cover the magnetic anomaly linear strip 9-6A region on the western side of the PVB, with depths ranging from 2000 to 6200 m. The survey ship trackline cuts the KPR and extends eastward through the "Chaotic Terrain" (Figure 4). Based on the high-resolution multibeam bathymetry data, abyssal hills arranged in regular linear patterns, V-shaped pseudo faults, and OCCs are clearly recognized (Figure 4). Based on magnetic anomaly data and seafloor topography trends, these features are part of the seafloor morphology formed during the E–W spreading stage of the PVB [21,45].

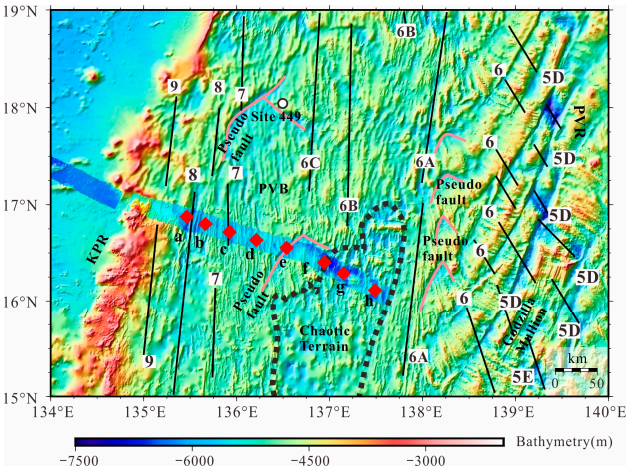


Figure 4. Distribution of magnetic anomaly linear strips and seafloor structural units in the western PVB. Tectonic units in the PVB and newly acquired multibeam bathymetry data are shown in the figure. The white circle represents the drilling site 449 of the DSDP 449 [46], red dots mark the locations of data blocks (a–h) in the study area, and the pink solid line represents V-shaped pseudo faults. The black dashed line represents the Chaotic Terrain, and the multibeam bathymetry ship trackline is plotted over the base map constructed using the GEBCO 2024 data [39]. The magnetic anomaly linear strip 9-6A [22] is shown on the western side of the PVB, where well-developed and regularly arranged abyssal hills are present. The multibeam bathymetry ship trackline crosses through the abyssal hills and the "Chaotic Terrain". The distribution of magnetic anomaly linear strips in the PVB are marked in the figure, and data are from [34], Magnetic Anomaly Map of East and Southeast Asia, Revised Version, 3rd Edition. The magnetic anomaly linear strips data are referenced from [22,35]. KPR: Kyushu-Palau Ridge; PVB: Parece Vela Basin; PVR: Parece Vela Rift.

Linear abyssal hills are mainly distributed in the western segment of the PVB, displaying clear and regular linear topographic features (Figure 5). High-resolution topographic data indicate that during the basin spreading, the abyssal hills near the KPR show the NNE–SSW orientation (Figure 5b). As spreading continued, the orientation began to shift to the N–S (Figure 5c). In the "Chaotic Terrain" area, the orientation of abyssal hills changes again to the NNE–SSW (Figure 5e), and this implies the instability of seafloor spreading on both the west and east segments. The PVB experienced two main spreading stages. The first was the E–W spreading [21,45]. However, the varying orientations of abyssal hills suggest that the first spreading stage was not entirely E–W and may involve local ridge reorientation adjustments (Figure 5). The widths of abyssal hills decrease from the west to the east, and this may likely relate to uneven magma supply during spreading in the PVB. According to the classic rift propagation model [47], unique V-shaped structural tracks (later named as V-shaped pseudo faults) are formed at off-axis locations during the ridge propagation. The appearance of similar V-shaped pseudo faults in the Atlantic ridge confirmed that magma supply variations are crucial to their propagation [48,49]. Using the seismic and gravity data, the formation and propagation of pseudo faults are confirmed to be closely linked to increased magma supply in surrounding spreading segments [50]. In the PVB, linear abyssal hills are distributed on both sides of the "Chaotic Terrain" in the PVB (Figure 6). The V-shaped pseudo faults (Figure 5c) and the bending of abyssal hills near the "Chaotic Terrain" (Figure 5e) support that the complex local tectonic activity is associated with the ridge propagation and jumps [21].

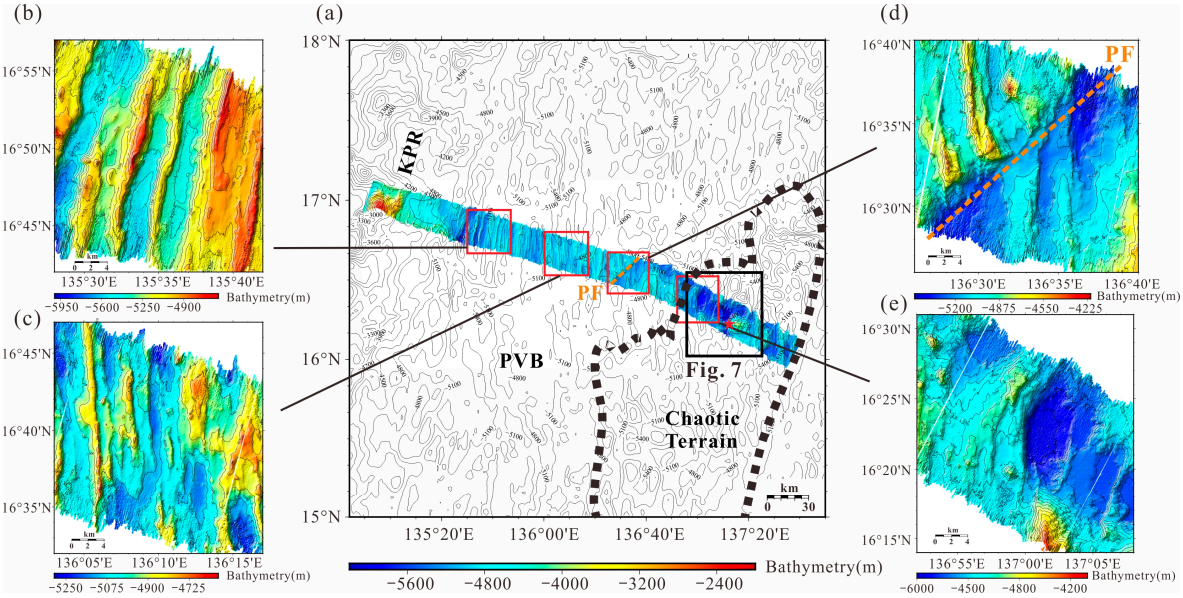


Figure 5. Topographic variations of linear abyssal hills in the PVB. (**a**) Multibeam bathymetry ship trackline in the PVB. The red star marks the dredging location of recovered peridotite and basalt (dredging location from [12]). (**b**) Seafloor topography of the NNE–SSW-oriented abyssal hills. (**c**) Seafloor topography of near the N–S-oriented abyssal hills. (**d**) Seafloor topography of near the N–S-oriented abyssal hills and pseudo faults. (**e**) Seafloor topography of the NNE–SSW-oriented abyssal hills and swales. Most abyssal hills are located in the western and central parts of the multibeam bathymetry strip. During the spreading process, the orientation of the abyssal hills gradually shifted from the NNE–SSW to near the N–S. At 136°35′ E, the abyssal hills are notably offset at the pseudo faults, and the subsequent ridge changes the orientation to the NNE–SSW with the decrease in width and the appearance of swales. KPR: Kyushu-Palau Ridge. PF: pseudo fault; PVB: Parece Vela Basin.

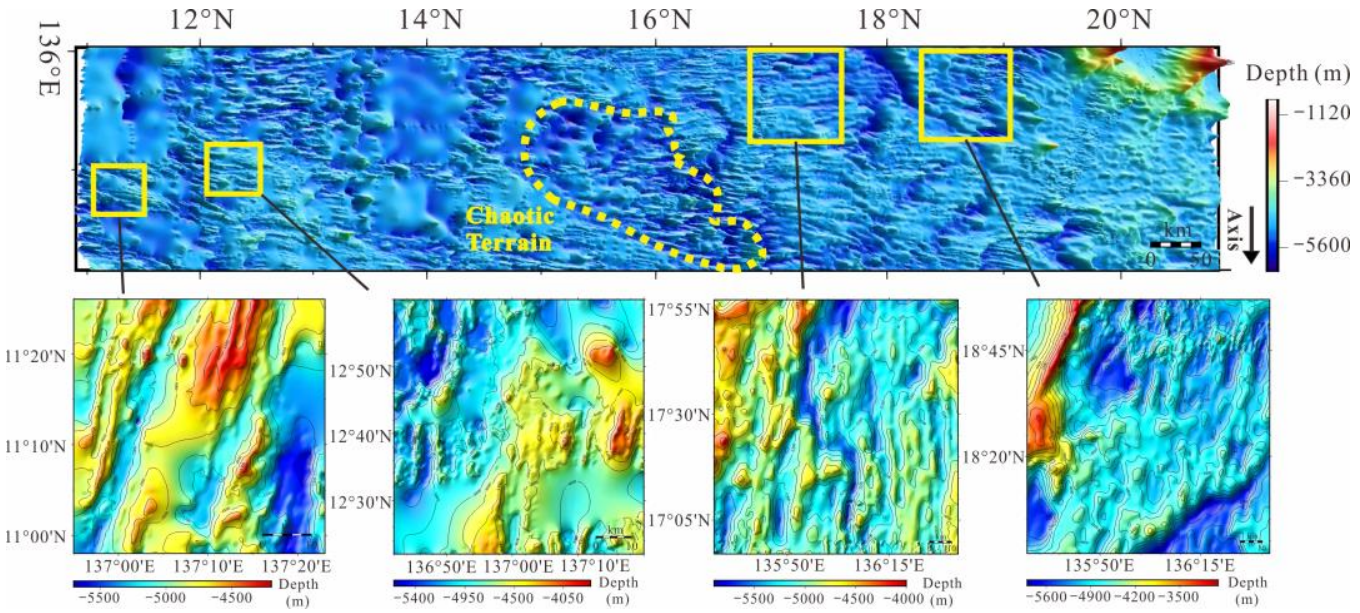


Figure 6. Seafloor topography of linear abyssal hills on the western side of the PVB. In the upper panel, large and linearly arranged abyssal hills are shown in the west of the PVB (based on GEBCO 2024 data [39]). The yellow dashed line marks the range of "Chaotic Terrain" composed of ridges and swales near ~16° N. Yellow boxes show locations that are illustrated in greater detail in the lower panel. In the lower panel, the enlarged seafloor topography is shown, and the detailed locations are shown in the yellow boxes in the upper panel.

In the eastern segment of the multibeam bathymetry coverage area (Figure 5), three OCCs (OCC-1, OCC-2, OCC-3) and four associated deep swales (S1–S4) (elongated depressions on the seafloor) are identified from the processed multibeam bathymetry data (Figure 7). The OCC-1 in the "Chaotic Terrain" is fully covered and shown in the multibeam bathymetry data (Figure 7). The recovered peridotite and basalt samples in the "Chaotic Terrain" [12] are consistent with global OCC rock characteristics [6,8]. Among them, deep swale S4 is the deepest point in the "Chaotic Terrain" with a depth of about 6200 m, and the elevation difference between the OCC and the swale is ~3680 m (Figure 7). In Figure 6, a typical corrugated surface is observed above the three isolated OCCs, and the corrugation surface is parallel to the spreading direction of the PVB. The OCC-1 shows a dome shape, about 2400 m in height and with an average 16.6 km in diameter (Figure 7). Two smaller OCCs (OCC-2 and OCC-3) are located alongside the OCC-1, and they show a linear distribution and are roughly parallel to the spreading direction of the PVB. The distribution pattern of OCCs in the PVB is highly similar to OCCs found in the Atlantic Ridge [51,52], Southwest Indian Ridge [8], and the Australian-Antarctic Discordance [11]. Typical OCCs on the Atlantic Ridge have a long axis extending approximately 5–10 km, while the OCC-1 in the "Chaotic Terrain" of the PVB is larger in scale and with a more rounded shape (diameter of ~16.6 km). According to the theory of regional balanced compensation, when a single detachment fault extends beyond 5 km, the formed OCC typically indicates a domed shape [6,51]. Therefore, the formation of OCCs in the "Chaotic Terrain" of the PVB may be related to long-lived detachment faulting.

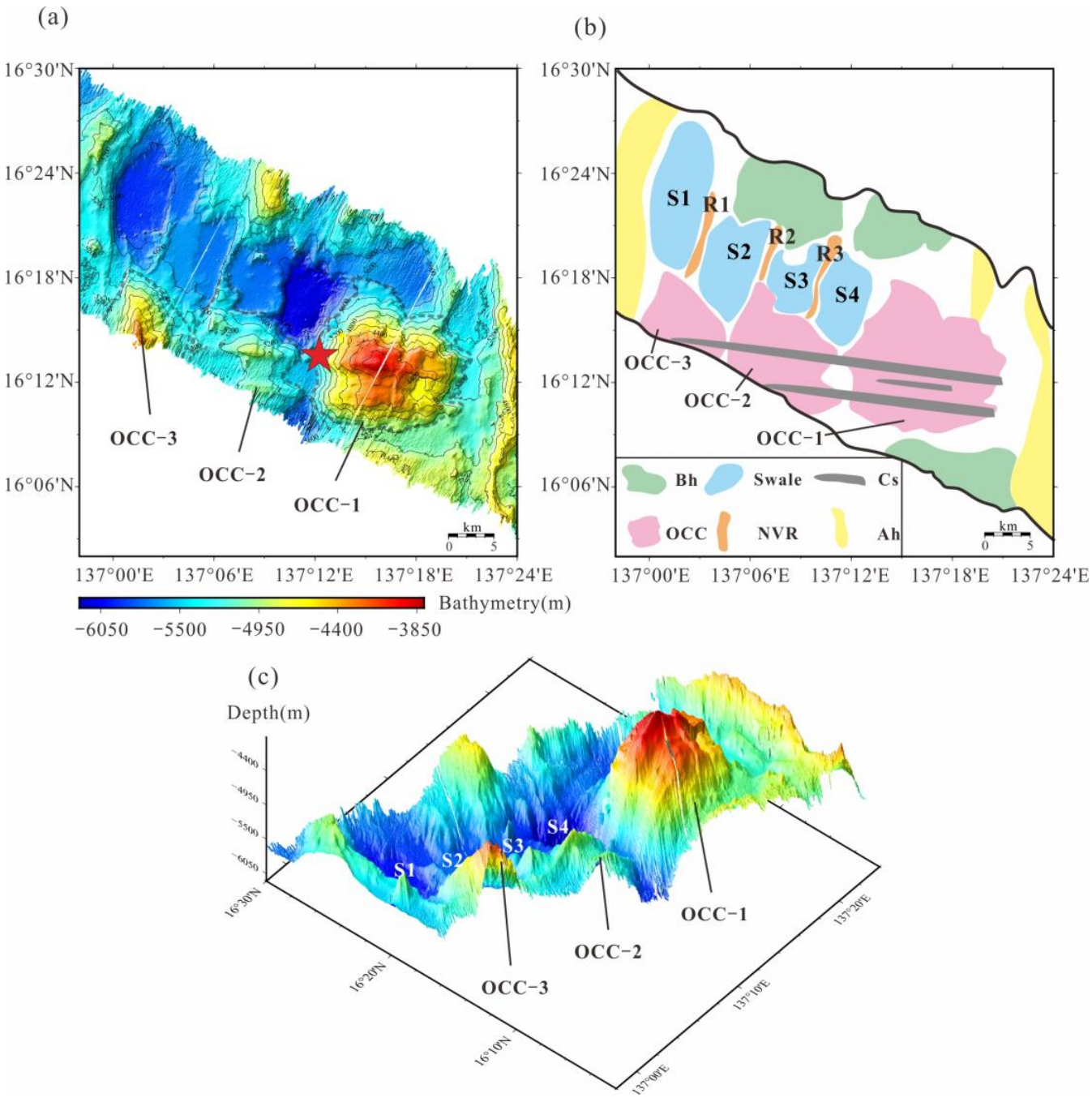


Figure 7. Topographic features and interpretation of three OCCs developed in the "Chaotic Terrain". (**a**) Seafloor topography of OCCs in the "Chaotic Terrain" region. The contour interval on the map is 200 m. The gray dashed lines outline three identified OCCs. The largest OCC (OCC-1) has a diameter of ~16.6 km. "R" represents the ridge-like topography, and it implies the separation of detachment surfaces. The red star marks the location of recovered peridotite and basalt (dredging location from [12]). S1–S4: Swale 1–Swale 4. (**b**) Three-dimensional bathymetry view of OCCs and swales. The largest OCC-1 is nearly vertical to the seafloor, displaying a dome shape and a distinct corrugated surface. Ah: Abyssal hill; Bh: Bathymetric high; Cs: Corrugated surface; NVR: Narrow Volcanic Ridge; OCC: Oceanic core complex.

Among three OCCs, four swales (S1–S4) and three narrow ridge-like structures (R1–R3) are identified in the bathymetry data, and they are distinct from the regularly arranged abyssal hills in the western segment (Table 1) (Figure 7). Near 137° E, the abyssal hills become more elongated (Figure 5e). The formation of OCCs and swales suggests that

seafloor changes are closely linked to fluctuations in magma supply. Similar narrow ridge-like structures and swales have been identified between OCCs on the Atlantic Ridge [1], but the distribution density of these features is much lower than in the PVB. Small ridge structures often appear between adjacent swales around the OCCs, indicating the onset of a new detachment event [51]. Based on the above analysis, the closely spaced and interconnected distribution of OCC-1, OCC-2, and OCC-3 in the "Chaotic Terrain" of the PVB is likely related to three consecutive detachment events.

Table 1. Location and depth variations of OCCs and swales.

Name of OCCs and Swales	Longitude (°E)	Latitude (°N)	Depth Range (m)
OCC-1	137.27250	16.21771	−3857~−5800
OCC-2	137.14400	16.21511	−4841~−5600
OCC-3	137.02400	16.25729	−4206~−5600
S1	137.03570	16.35339	−7307~−5998
S2	137.09730	16.32089	−5557~−5800
S3	137.13750	16.29494	−5415~−5996
S4	137.19340	16.27157	−5725~−6200

4.2. Relationship Between Linear Seafloor Topography and Magma Supply

Two-dimensional discrete Fourier transform image analysis shows high sensitivity to linear topographic features. We selected eight data blocks (a–h) from the west to the east in the PVB covered by the multibeam bathymetry data, and we calculated the slope variations and linearity of the seafloor topography (Figure 4). The slope variations in the seafloor topography from different blocks (a to h) reveal significant differences in topographic linearity between the eastern and western segments of the data (Figure 8a–h). The slopes of abyssal hills mainly vary from 15° to 45°. From the slope maps, it is evident that the seafloor structure of blocks a to d shows higher linearity and lower seafloor roughness (Figure 8a–d), and they further suggest that there may be higher spreading rates or abundant magma supply in this region, where topographic changes are stable during the spreading. In block e, V-shaped pseudo faults are also identified with about a 2 km offset between the faults and the adjacent abyssal hills. Compared to blocks a to d, abyssal hills in block e are significantly wider and the widths are up to 2 km (Figure 8e). Blocks f to h are located within the "Chaotic Terrain" of the PVB, and they show significantly lower topographic linearity than blocks a to d. This may show the complex and intense tectonic activity during the spreading process, leading to the uneven distribution of seafloor topography in the eastern and western segments.

After 2D discrete Fourier image processing, the intensity function results of the eight data blocks are obtained (Figure 9). From blocks a to d, the AR values fluctuate between 1.7 and 2.1, especially after the orientation of abyssal hills shifts from the NNE–SSW to the N–S, where the AR value increases from 1.9 to 2.1 (Figure 9a,b). This variation suggests that the increase in magma supply in block b may be linked to changes in orientation of abyssal hills. As spreading continued, AR values of abyssal hills with a nearly N–S orientation are gradually stable at 1.7 (Figure 9c,d). This indicates the relatively stable magma supply and a gradual spreading process. The AR values increase to 2.1 at the pseudo fault (Figure 9e). This may indicate that the early steady-state spreading balance was disrupted, and the increase in magma supply could be linked to a past ridge propagation event in this region [12,21]. Obviously, as spreading progressed, the western segment of the multibeam trackline shows significantly different AR values compared to the eastern segment of the multibeam trackline. From blocks f to g, AR values decrease sharply to 1.3 (Figure 9f,g), and this may be linked to reduced magma supply and multiple OCCs appearing in this

region. The AR value variations imply that the formation of OCCs in the "Chaotic Terrain" is closely related to reduced magma supply, rather than the result of the amagmatic process (intermittent magma supply). The region with the AR values of 1.3 suggests that, despite low magma supply, detachment activity persists long enough to form a large-scale OCC-1 with a diameter of approximately 16.6 km [13,15,51]. After the formation of the OCC-1, the AR values in block h increase to 1.9, indicating an increase in magma supply during the later stages of spreading process (Figure 9e). The AR value variations clearly reveal a positive correlation between the linearity of seafloor topography textures in the slope from the grayscale maps and magma supply.

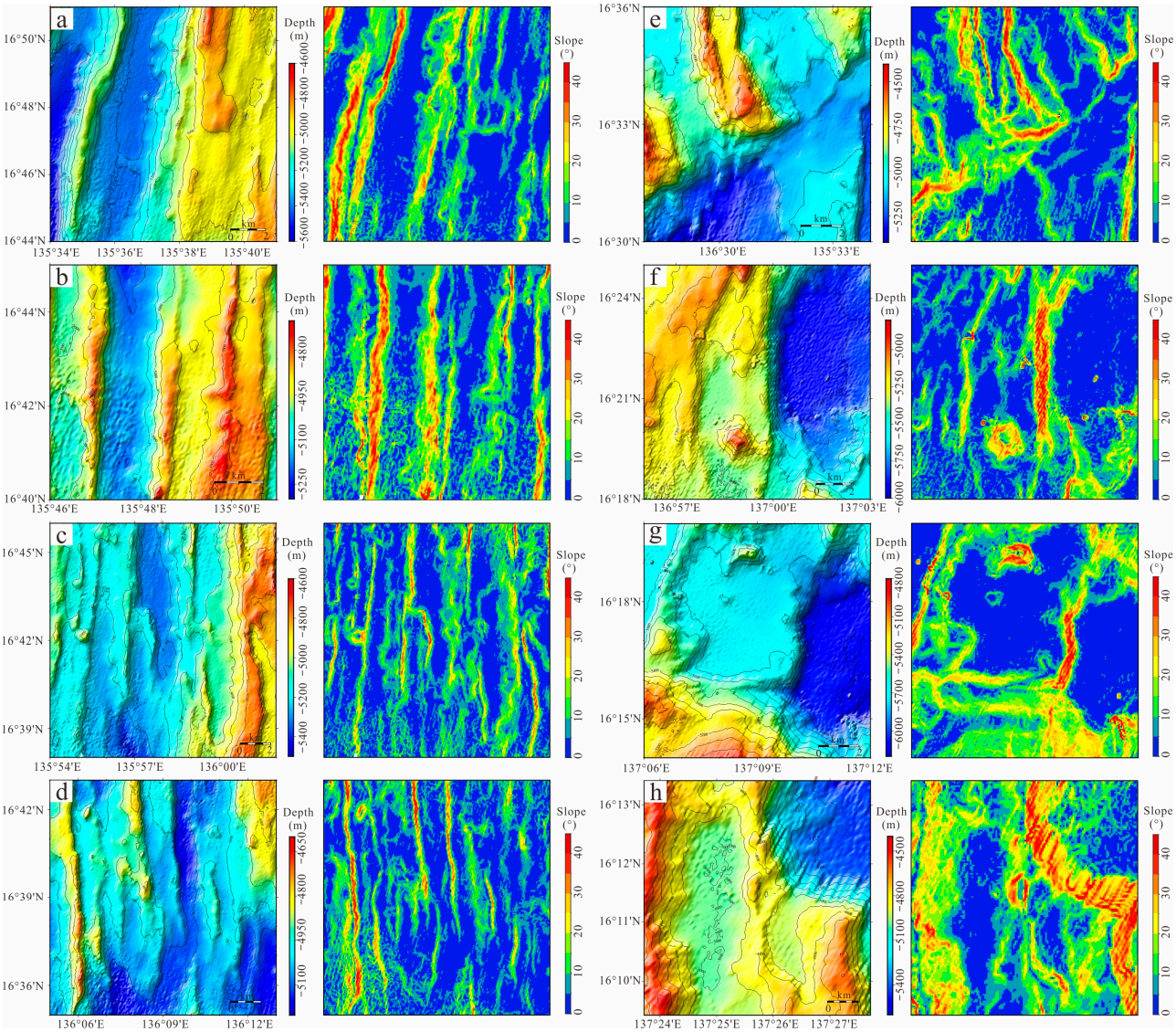


Figure 8. Seafloor topography and slope variations of eight data block pairs in the PVB. The seafloor topography is shown in the left column, and the slope is shown in the right column. The seafloor slope of (**a**–**h**) data blocks mainly range from 5° to 20°, while in the region with abyssal hills, the slope varies from 15° to 45°. The topographic map clearly shows the linearity and directional changes of the seafloor topography associated with spreading. The locations of eight data block pairs (**a**–**h**) are shown in Figure 4.

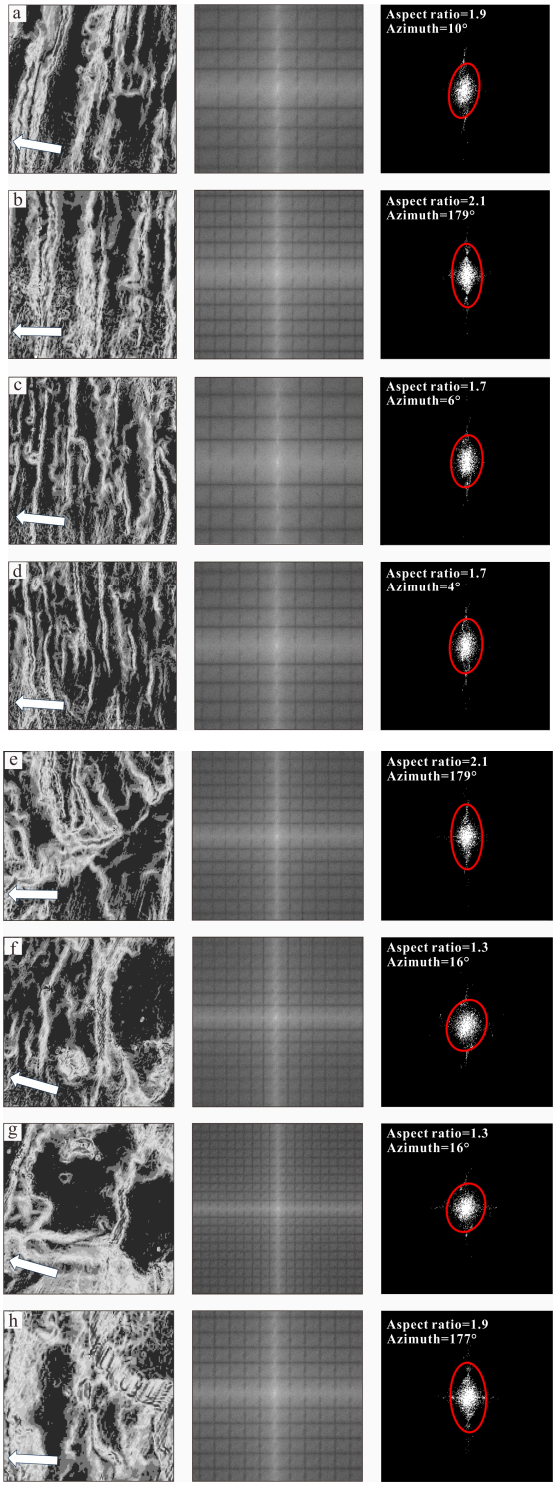


Figure 9. Two-dimensional discrete Fourier image calculation of eight data blocks in the PVB. The first column images (**a**–**h**) show the slope grayscale images generated with 600 dpi resolution. White arrows indicate the calculated spreading direction. The second column images (**a**–**h**) present the spectrum derived from the grayscale images, and the third column images (**a**–**h**) show the binarized result of the spectrum (white dots). To estimate the AR, red ellipses are drawn using the same centroid position, semi-major axis, and semi-minor axis lengths. When the AR values are larger than 1.5, the ellipse's orientation reflects the short axis direction. When the AR values are lower than 1.5, the orientation indicates the long axis direction [44]. Eight data blocks were selected along the multibeam bathymetry ship trackline, and 2D discrete Fourier transform was used to obtain the spectral characteristics and the AR values. The locations of data blocks are shown in Figure 4.

The magnetic anomaly linear strip 9-6A region of the PVB, has been summarized as the first spreading stage (E–W spreading) by previous studies [21,45]. However, based on the spreading directions obtained from 2D discrete Fourier image analysis, the spreading direction shifts from NWW–SEE to E–W. Then, it reverts to the NWW–SEE near the "Chaotic Terrain". After the formation of the "Chaotic Terrain", the spreading direction turns back to approximately the E–W (Figure 9). The spreading variations indicate the dynamic change in the spreading process. When the spreading direction change is small and limited, the spreading axis is more likely to undergo a jump or rotational reorientation process [53]. In the first spreading stage of the PVB, the magnetic anomaly linear strips in the western basin are not perfectly parallel to the north–south direction, but instead show the slight rotation (Figure 4). Based on the 2D Fourier image analysis, we propose that the first spreading stage of the PVB not only experienced the ridge propagation reorientation near the "Chaotic Terrain" but may have also undergone ridge rotation reorientation in the early spreading stage [32,47,54].

4.3. Development Mechanism and Process of the "Chaotic Terrain" in the PVB

The "Chaotic Terrain" in the PVB is composed of a series of OCCs, forming a patchy block [12,17]. In this study we integrate the high-resolution multibeam bathymetry data, magnetic anomaly data, and 2D discrete Fourier analysis to investigate detachment faults and OCCs found in the "Chaotic Terrain". Based on the relationship between these structural features and magma supply, it is observed that the PVB underwent the ridge reorientation during the early spreading stages, with the magma supply first decreasing and then increasing. The distribution of OCCs and the detachment faulting in the Parece Vela Basin indicates the low magma supply, consistent with findings of OCCs in other global mid-ocean ridges [11,55–57]. In the eastern Southwest Indian Ridge, several OCCs with diameters of 10–12 km were found in areas of low magma supply [55]. Atlantis Bank (AB, location see in Figure 1a) in the Southwest Indian Ridge, a typical OCC with a diameter of ~20 km, is shaped by long-term detachment faulting [56]. An OCC with a diameter of ~18 km in the N2 segment of the Atlantic Ridge is also influenced by detachment faulting and low magma supply [57]. OCCs with diameters of 10–20 km have been observed at the Australian-Antarctic Discordance, where the low magma supply was reported [11], similar to the OCC-1 in the Parece Vela Basin (diameter ~16.6 km) in this study. Therefore, the formation of large-scale OCCs is closely linked to persistent detachment faulting and low magma supply.

We propose that the spreading process in the magnetic anomaly linear strips 9-6A of the PVB are summarized into four evolution stages (Figure 10). At the first stage, normal faults show the normal ridge spreading process (Figure 10a) and the orientation of the abyssal hills shifted from the NNE–SSW to the N–S, accompanied by the development of normal faults. The magma supply shows minor fluctuations (AR values between 1.7 and 2.1), and it indicates a stable spreading process. At the second stage, it is involved in ridge propagation (Figure 10b), and typical V-shaped pseudo faults were formed. The 2D discrete Fourier analysis shows that the AR values increase to 2.1, and this may be related to the ridge propagation, followed by the onset of detachment faults. The third stage represents a stage of poor magma supply (Figure 10c), where a new spreading center appeared on the western side of the PVB. However, due to the northward propagation of the main spreading center in the east of the new spreading center, the new spreading center quickly ceased activity at this stage [21]. At the third stage, the AR values decrease to 1.3, and it was followed by the development of detachment faults and the formation of OCCs. At the fourth stage, it is characterized by the maturation development of OCCs and the formation of the "Chaotic Terrain" with the magma supply increasing to the first stage

levels. The spreading direction began to shift from the NNE–SSW to near the E–W, and the later formed spreading center began to rotate counterclockwise, entering the NE–SW spreading stage (Figure 10d).

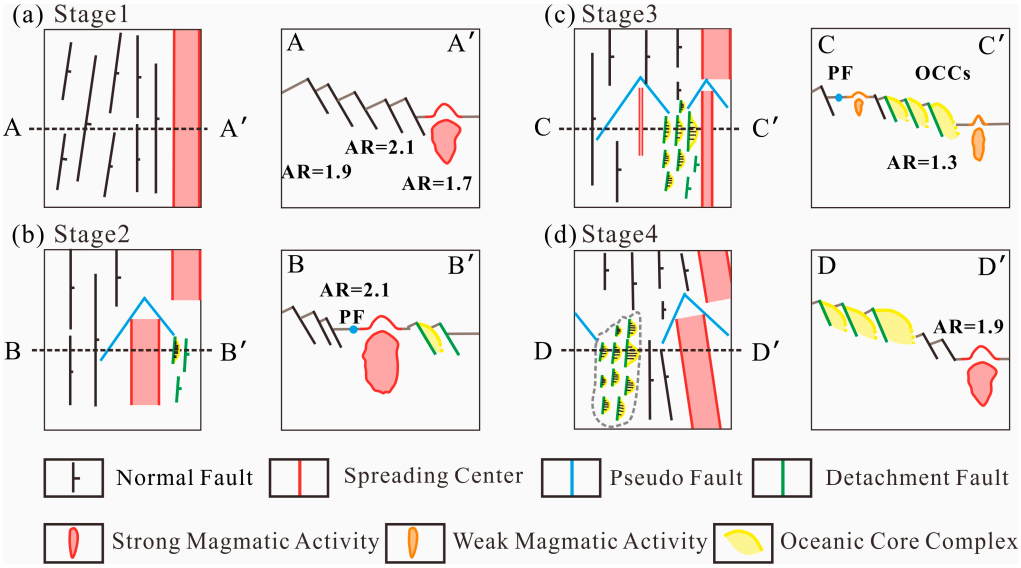


Figure 10. Development mechanism and spreading process of abyssal hills and OCCs in the "Chaotic Terrain" of the PVB. (**a**) Stage 1: Ridge rotation stage. During the spreading the orientation of abyssal hills shifted from the NNE–SSW to the N–S. (**b**) Stage 2: Ridge propagation stage. Detachment faults begin to form, with the formation of typical V-shaped pseudo faults accompanied by ridge propagation, inducing the N–S abyssal hills to the NNE–SSW direction. (**c**) Stage 3: The poor magma supply stage is marked by a series of detachment faults, and OCCs gradually formed in the "Chaotic Terrain". (**d**) Stage 4: Maturation stage of OCCs. OCCs were combined to form the "Chaotic Terrain" with abyssal hills shifting from the NNE–SSW to the N-S direction, followed by the transition into the NE–SW spreading stage. OCCs: Oceanic core complexes; PF: pseudo fault. In each pair, the left is map view, while the right is the cross-sectional view.

5. Conclusions

Based on the multibeam bathymetry data acquired in 2023 and regional magnetic anomaly data from the extinct mid-ocean ridge system in the PVB, we systematically investigate seafloor topography variations of abyssal hills and OCCs and construct the spreading process model of the PVB in the magnetic anomaly linear strip 9-6A segment. With fine multibeam bathymetry data processing and the 2D discrete Fourier image analysis, we examine the ridge reorientation and OCC formation during the spreading process in the PVB. The following important conclusions are drawn from the comprehensive analysis:

(1) During the spreading of the PVB, the orientation of abyssal hills shifted from the NNE–SSW to the N–S, and it indicates the typical ridge rotation reorientation. As the spreading process continued, the abyssal hills at the "Chaotic Terrain" changed again from the N–S to the NNE–SSW, accompanied by the formation of typical V-shaped pseudo faults. Seafloor topography variations represent ridge propagation reorientation.

(2) Based on the calculated AR values from the linear seafloor topography of the PVB, magma supply is greatly imbalanced during the spreading process of the PVB. The magma supply and topographic linearity in the abyssal hill region were much higher than in the "Chaotic Terrain" region. During the early stages of spreading, AR values fluctuated between 2.1 and 1.7 for abyssal hills in the western segment. In the "Chaotic Terrain" region, the magma supply significantly decreased, and the AR values decreased to 1.3. After the formation of OCC-1, AR values increased to 1.9 in the eastern segment,

and this shows that the magma supply increases. The formation of OCC-1, OCC-2, and OCC-3 in the "Chaotic Terrain" is mainly related to reduced magma supply and three continuous detachment faults. Based on the seafloor topography variations and magma supply changes during the spreading process, we propose that the spreading process of the PVB in the magnetic anomaly linear strip 9-6A segment underwent four main stages: ridge rotation, ridge propagation, magma-poor supply, and the maturation of OCCs.

Author Contributions: Conceptualization, X.D.; methodology, X.D.; software, X.D.; validation, J.Z.; formal analysis, X.L. and Y.J.; investigation, X.D. and Y.H.; resources, J.Z.; data curation, Y.J., Z.L. and X.A.; writing—original draft preparation, X.D.; writing—review and editing, J.Z.; visualization, X.D.; supervision, J.Z. and S.L.; project administration, J.Z.; funding acquisition, J.Z. All authors have read and agreed to the published version of the manuscript.

Funding: This study has been supported by the National Natural Science Foundation of China (42276058), the Laoshan Laboratory (LSKJ 202201701), and the Fundamental Research Funds for the Central Universities (202372001; 202172002).

Data Availability Statement: The data that support the findings of this study are available from the corresponding author upon reasonable request.

Acknowledgments: We would like to acknowledge the crew, scientists, and technicians of the R/V "Dongfanghong 3" for their work during the data collection in 2023. We used the GMT 6.4 software [58] plot several figures. We also thank the global bathymetry dataset GEBCO Compilation Group (2024) GEBCO 2024 Grid (https://doi.org/10.5285/1c44ce99-0a0d-5f4f-e063-7086abc0ea0f, accessed on 9 July 2025).

Conflicts of Interest: The authors declare no conflicts of interest.

References

1. Smith, D.K.; Cann, J.R.; Escartín, J. Widespread Active Detachment Faulting and Core Complex Formation near 13° N on the Mid–Atlantic Ridge. *Nature* **2006**, *442*, 440–443. [CrossRef]
2. Blackman, D.K.; Cann, J.R.; Janssen, B.; Smith, D.K. Origin of Extensional Core Complexes: Evidence from the Mid-Atlantic Ridge at Atlantis Fracture Zone. *J. Geophys. Res. Solid Earth* **1998**, *103*, 21315–21333. [CrossRef]
3. Tucholke, B.E.; Lin, J.; Kleinrock, M.C. Megamullions and Mullion Structure Defining Oceanic Metamorphic Core Complexes on the Mid-Atlantic Ridge. *J. Geophys. Res. Solid Earth* **1998**, *103*, 9857–9866. [CrossRef]
4. Ciazela, J.; Koepke, J.; Dick, H.J.B.; Muszynski, A. Mantle Rock Exposures at Oceanic Core Complexes along Mid–Ocean Ridges. *Geologos* **2015**, *21*, 207–231. [CrossRef]
5. Mrozowski, C.L.; Hayes, D.E. The Evolution of the Parece Vela Basin, Eastern Philippine Sea. *Earth Planet. Sci. Lett.* **1979**, *46*, 49–67. [CrossRef]
6. Buck, W.R. Flexural Rotation of Normal Faults. *Tectonics* **1988**, *7*, 959–973. [CrossRef]
7. Ohara, Y.; Yoshida, T.; Kato, Y.; Kasuga, S. Giant Megamullion in the Parece Vela Backarc Basin. *Mar. Geophys. Res.* **2001**, *22*, 47–61. [CrossRef]
8. Cannat, M.; Sauter, D.; Mendel, V.; Ruellan, E.; Okino, K.; Escartin, J.; Combier, V.; Baala, M. Modes of Seafloor Generation at a Melt–Poor Ultraslow–Spreading Ridge. *Geology* **2006**, *34*, 605. [CrossRef]
9. Mitchell, N.; Escartin, J.; Allerton, S. Detachment Faults at Mid-Ocean Ridges Garner Interest. *Eos Trans. Am. Geophys. Union* **1998**, *79*, 127. [CrossRef]
10. Feng, B.; Li, J.; Tao, C.; Liu, C. Magmatic and tectonic crustal accretion at the Southwest Indian Ridge between 49°E and 52°E. *Chin. J. Geophys.* **2024**, *67*, 4733–4747. [CrossRef]
11. Okino, K.; Matsuda, K.; Christie, D.M.; Nogi, Y.; Koizumi, K. Development of Oceanic Detachment and Asymmetric Spreading at the Australian-Antarctic Discordance. *Geochem. Geophys. Geosyst.* **2004**, *5*, Q12012. [CrossRef]
12. Ohara, Y.; Okino, K.; Kasahara, J. Seismic Study on Oceanic Core Complexes in the Parece Vela Back–Arc Basin. *Isl. Arc* **2007**, *16*, 348–360. [CrossRef]
13. Buck, W.R.; Lavier, L.L.; Poliakov, A.N.B. Modes of Faulting at Mid–Ocean Ridges. *Nature* **2005**, *434*, 719–723. [CrossRef] [PubMed]
14. Ildefonse, B.; Blackman, D.; John, B.E.; Ohara, Y.; Macleod, C.J.; Andreani, M. Oceanic Core Complex and Crustal Accretion a Slow–Spreading Ridges. *Geology* **2007**, *35*, 623–626. [CrossRef]

15. MacLeod, C.J.; Searle, R.C.; Murton, B.J.; Casey, J.F.; Mallows, C.; Unsworth, S.C.; Achenbach, K.L.; Harris, M. Life Cycle of Oceanic Core Complexes. *Earth Planet. Sci. Lett.* **2009**, *287*, 333–344. [CrossRef]
16. Tucholke, B.E.; Behn, M.D.; Buck, W.R.; Lin, J. Role of Melt Supply in Oceanic Detachment Faulting and Formation of Megamullions. *Geology* **2008**, *36*, 455–458. [CrossRef]
17. Ohara, Y.; Fujioka, K.; Ishii, T.; Yurimoto, H. Peridotites and Gabbros from the Parece Vela Backarc Basin: Unique Tectonic Window in an Extinct Backarc Spreading Ridge. *Geochem. Geophys. Geosyst.* **2003**, *4*, 8611. [CrossRef]
18. Ohara, Y.; Okino, K.; Snow, J.E. Tectonics of Unusual Crustal Accretion in the Parece Vela Basin. In *Accretionary Prisms and Convergent Margin Tectonics in the Northwest Pacific Basin*; Ogawa, Y., Anma, R., Dilek, Y., Eds.; Springer: Dordrecht, The Netherlands, 2011; pp. 149–168. [CrossRef]
19. Nishizawa, A.; Kaneda, K.; Oikawa, M. Crust and Uppermost Mantle Structure of the Kyushu–Palau Ridge, Remnant Arc on the Philippine Sea Plate. *Earth Planets Space* **2016**, *68*, 30. [CrossRef]
20. Whitney, D.L.; Teyssier, C.; Rey, P.; Buck, W.R. Continental and Oceanic Core Complexes. *Geol. Soc. Am. Bull.* **2013**, *125*, 273–298. [CrossRef]
21. Okino, K.; Kasuga, S.; Ohara, Y. A New Scenario of the Parece Vela Basin Genesis. *Mar. Geophys. Res.* **1998**, *20*, 21–40. [CrossRef]
22. Sdrolias, M.; Roest, W.R.; Müller, R.D. An Expression of Philippine Sea Plate Rotation: The Parece Vela and Shikoku Basins. *Tectonophysics* **2004**, *394*, 69–86. [CrossRef]
23. Loocke, M.; Snow, J.E.; Ohara, Y. Melt Stagnation in Peridotites from the Godzilla Megamullion Oceanic Core Complex, Parece Vela Basin, Philippine Sea. *Lithos* **2013**, *182–183*, 1–10. [CrossRef]
24. Sanfilippo, A.; Dick, H.J.B.; Ohara, Y. Melt–Rock Reaction in the Mantle: Mantle Troctolites from the Parece Vela Ancient Back–Arc Spreading Center. *J. Petrol.* **2013**, *54*, 861–885. [CrossRef]
25. Gong, X.; Tian, L.; Dong, Y. Contrasting Melt Percolation and Melt–Rock Reactions in the Parece Vela Back–Arc Oceanic Lithosphere, Philippine Sea: A Mineralogical Perspective. *Lithos* **2022**, *422–423*, 106727. [CrossRef]
26. Ohara, Y.; Kasuga, S.; Ishii, T. Peridotites from the Parece Vela Rift in the Philippine Sea. *Proc. Jpn. Acad. Ser. B* **1996**, *72*, 118–123. [CrossRef]
27. Kasuga, S.; Ohara, Y. A New Model of Back–Arc Spreading in the Parece Vela Basin, Northwest Pacific Margin. *Isl. Arc* **1997**, *6*, 316–326. [CrossRef]
28. Harigane, Y.; Michibayashi, K.; Ohara, Y. Amphibolitization within the Lower Crust in the Termination Area of the Godzilla Megamullion, an Oceanic Core Complex in the Parece Vela Basin. *Isl. Arc* **2010**, *19*, 718–730. [CrossRef]
29. Ohara, Y. The Godzilla Megamullion, the largest oceanic core complex on the earth: A historical review. *Isl. Arc* **2016**, *25*, 193–208. [CrossRef]
30. Olive, J.-A.; Behn, M.D.; Tucholke, B.E. The Structure of Oceanic Core Complexes Controlled by the Depth Distribution of Magma Emplacement. *Nat. Geosci.* **2010**, *3*, 491–495. [CrossRef]
31. Nishizawa, A.; Kaneda, K.; Katagiri, Y.; Kasahara, J. Variation in Crustal Structure along the Kyushu–Palau Ridge at 15–21°N on the Philippine Sea Plate Based on Seismic Refraction Profiles. *Earth Planets Space* **2007**, *59*, e17–e20. [CrossRef]
32. Menard, H.W.; Atwater, T. Changes in Direction of Sea Floor Spreading. *Nature* **1968**, *219*, 463–467. [CrossRef]
33. Zhang, F.; Wang, D.; Ji, X.; Hou, F.; Yang, Y.; Wang, W. Structural Features in the Mid–Southern Section of the Kyushu–Palau Ridge Based on Satellite Altimetry Gravity Anomaly. *Acta Oceanol. Sin.* **2024**, *43*, 50–60. [CrossRef]
34. Ishihara, T.; Uchida, T. *Magnetic Anomaly Map of East and Southeast Asia, Revised Version (3rd Edition), Explanatory Note*; Geological Survey of Japan: Tsukuba, Japan, Digital Geoscience Map P-3, Revised; 2021; pp. 1–14.
35. Xu, S.; Ye, Q.; Li, S.; Somerville, I.; Feng, H.; Tang, Z.; Shu, D.; Bi, H. Sequential Patterns in Cenozoic Marginal Basins of the Northwest Pacific. *Geol. J.* **2016**, *51*, 387–415. [CrossRef]
36. Kongsberg Maritime. *Kongsberg EM122 Multibeam Echo Sounder Maintenance Manual*; Kongsberg Maritime: Navi Mumbai, India, 2009.
37. Universal System. In *CARIS HIPS&SIPS User Guide*; 2013; pp. 1–542.
38. Chen, X.; Zhu, J.; Jiao, Y.; Ding, X.; Zhu, Q.; Liu, Z.; Li, S.; Jia, Y.; Liu, Y. Geomorphological Features and Formation Mechanism of the Taixinan Canyon-channel System in the North-eastern South China Sea. *Geol. J.* **2025**, *60*, 290–310. [CrossRef]
39. GEBCO Compilation Group. GEBCO 2024 Grid. Available online: https://www.gebco.net/data-products-gridded-bathymetry-data/gebco2024-grid (accessed on 9 July 2025).
40. Jenness, J. DEM Surface Tools. Jenness Enterprises. Available online: http://www.jennessent.com/arcgis/surface_area.htm (accessed on 9 July 2025).
41. Burrough, P.A.; McDonnell, R.A.; Lloyd, C.D. *Principles of Geographical Information Systems*; OUP Oxford: Oxford, UK, 2015.
42. Horn, B.K.P. Hill Shading and the Reflectance Map. *Proc. IEEE* **1981**, *69*, 14–47. [CrossRef]
43. Hodgson, M.E. What Cell Size Does the Computed Slope/Aspect Angle Represent? *Photogramm. Eng. Remote Sens.* **1995**, *61*, 513–517. [CrossRef]

44. Tucholke, B.E.; Parnell-Turner, R.; Smith, D.K. The Global Spectrum of Seafloor Morphology on Mid-Ocean Ridge Flanks Related to Magma Supply. *J. Geophys. Res. Solid Earth* **2023**, *128*, e2023JB027367. [CrossRef]
45. Okino, K.; Ohara, Y.; Kasuga, S.; Kato, Y. The Philippine Sea: New Survey Results Reveal the Structure and the History of the Marginal Basins. *Geophys. Res. Lett.* **1999**, *26*, 2287–2290. [CrossRef]
46. Mattey, D.P.; Marsh, N.G.; Tarney, J. The Geochemistry, Mineralogy, and Petrology of Basalts from the West Philippine and Parece Vela Basins and from the Palau–Kyushu and West Mariana Ridges, Deep Sea Drilling Project Leg 59. In *Initial Reports of the Deep Sea Drilling Project*; U.S. Government Printing Office: Washington, DC, USA, 1981; Volume 59, pp. 753–800. [CrossRef]
47. Hey, R. A New Class of "Pseudofaults" and Their Bearing on Plate Tectonics: A Propagating Rift Model. *Earth Planet. Sci. Lett.* **1977**, *37*, 321–325. [CrossRef]
48. Cannat, M.; Mevel, C.; Maia, M.; Deplus, C.; Durand, C.; Gente, P.; Agrinier, P.; Belarouchi, A.; Dubuisson, G.; Humler, E.; et al. Thin Crust, Ultramafic Exposures, and Rugged Faulting Patterns at the Mid–Atlantic Ridge (22°–24°N). *Geology* **1995**, *23*, 49–52. [CrossRef]
49. Zheng, T.; Tucholke, B.E.; Lin, J. Long-Term Evolution of Nontransform Discontinuities at the Mid-Atlantic Ridge, 24°N–27°30′N. *J. Geophys. Res. Solid Earth* **2019**, *124*, 10023–10055. [CrossRef]
50. Dannowski, A.; Morgan, J.P.; Grevemeyer, I.; Ranero, C.R. Enhanced Mantle Upwelling/Melting Caused Segment Propagation, Oceanic Core Complex Die Off, and the Death of a Transform Fault: The Mid–Atlantic Ridge at 21.5°N. *J. Geophys. Res. Solid Earth* **2018**, *123*, 941–956. [CrossRef]
51. Smith, D.K.; Escartín, J.; Schouten, H.; Cann, J.R. Fault Rotation and Core Complex Formation: Significant Processes in Seafloor Formation at Slow-spreading Mid-ocean Ridges (Mid-Atlantic Ridge, 13°–15°N). *Geochem. Geophys. Geosys.* **2008**, *9*, 2007GC001699. [CrossRef]
52. Smith, D.K.; Schouten, H.; Dick, H.J.B.; Cann, J.R.; Salters, V.; Marschall, H.R.; Ji, F.; Yoerger, D.; Sanfilippo, A.; Parnell-Turner, R.; et al. Development and Evolution of Detachment Faulting along 50 Km of the Mid-Atlantic Ridge near 16.5°N. *Geochem. Geophys. Geosyst.* **2014**, *15*, 4692–4711. [CrossRef]
53. Goodliffe, A.M.; Taylor, B.; Martinez, F.; Hey, R.; Maeda, K.; Ohno, K. Synchronous Reorientation of the Woodlark Basin Spreading Center. *Earth Planet. Sci. Lett.* **1997**, *146*, 233–242. [CrossRef]
54. Hey, R.N.; Menard, H.W.; Atwater, T.M.; Caress, D.W. Changes in Direction of Seafloor Spreading Revisited. *J. Geophys. Res. Solid Earth* **1988**, *93*, 2803–2811. [CrossRef]
55. Cannat, M.; Sauter, D.; Escartín, J.; Lavier, L.; Picazo, S. Oceanic Corrugated Surfaces and the Strength of the Axial Lithosphere at Slow Spreading Ridges. *Earth Planet. Sci. Lett.* **2009**, *288*, 174–183. [CrossRef]
56. Baines, A.G.; Cheadle, M.J.; John, B.E.; Schwartz, J.J. The Rate of Oceanic Detachment Faulting at Atlantis Bank, SW Indian Ridge. *Earth Planet. Sci. Lett.* **2008**, *273*, 105–114. [CrossRef]
57. Fujiwara, T.; Lin, J.; Matsumoto, T.; Kelemen, P.B.; Tucholke, B.E.; Casey, J.F. Crustal Evolution of the Mid-Atlantic Ridge near the Fifteen-Twenty Fracture Zone in the Last 5 Ma. *Geochem. Geophys. Geosyst.* **2003**, *4*, 1024. [CrossRef]
58. Wessel, P.; Smith, W.H.F. New, Improved Version of Generic Mapping Tools Released. *Eos Trans. Am. Geophys. Union* **1998**, *79*, 579. [CrossRef]

Disclaimer/Publisher's Note: The statements, opinions and data contained in all publications are solely those of the individual author(s) and contributor(s) and not of MDPI and/or the editor(s). MDPI and/or the editor(s) disclaim responsibility for any injury to people or property resulting from any ideas, methods, instructions or products referred to in the content.